Functional Evaluation of Conserved Basic Residues in Human Phosphomevalonate Kinase†

Timothy J. Herdendorf and Henry M. Miziorko*

Division of Molecular Biology & Biochemistry, School of Biological Sciences, University of Missouri−Kansas City, Kansas City, Missouri 64110

Received July 17, 2007; Revised Manuscript Received August 9, 2007

ABSTRACT: Phosphomevalonate kinase (PMK) catalyzes the cation-dependent reaction of mevalonate 5-phosphate with ATP to form mevalonate 5-diphosphate and ADP, a key step in the mevalonate pathway for isoprenoid/sterol biosynthesis. Animal PMK proteins belong to the nucleoside monophosphate (NMP) kinase family. For many NMP kinases, multiple basic residues contribute to the neutralization of the negatively charged pentacoordinate phosphate reaction intermediate. Loss of basicity can result in catalytically impaired enzymes. On the basis of this precedent, conserved basic residues of human PMK have been mutated, and purified forms of the mutated proteins have been kinetically and biophysically characterized. K48M and R73M mutants exhibit diminished V_{max} values in both reaction directions (>1000-fold) with only slight K_m perturbations (<10-fold). In both forward and reverse reactions, R110M exhibits a large (>10 000-fold) specific activity diminution. R111M exhibits substantially inflated K_m values for mevalonate 5-phosphate and mevalonate 5-diphosphate (60- and 30-fold, respectively) as well as decreases [50-fold (forward) and 85-fold (reverse)] in V_{max}. R84M also exhibits inflated K_m values (50- and 33-fold for mevalonate 5-phosphate and mevalonate 5-diphosphate, respectively). The K_i values for R111M and R84M product inhibition by mevalonate 5-diphosphate are inflated by 45- and 63-fold; effects are comparable to the 30- and 38-fold inflations in K_m for mevalonate 5-diphosphate. R141M exhibits little perturbation in V_{max} [14-fold (forward) and 10-fold (reverse)] but has inflated K_m values for ATP and ADP (48- and 136-fold, respectively). The K_d of ATP for R141M, determined by changes in tryptophan fluorescence, is inflated 27-fold compared to wt PMK. These data suggest that R110 is important to PMK catalysis, which is also influenced by K48 and R73. R111 and R84 contribute to binding of mevalonate 5-phosphate and R141 to binding of ATP.

Phosphomevalonate kinase (PMK;[1] EC 2.7.4.2) catalyzes the reversible ATP-dependent phosphorylation of mevalonate 5-phosphate to produce mevalonate 5-diphosphate and ADP:

mevalonate 5-phosphate + ATP ⇄ mevalonate 5-diphosphate + ADP

The reaction represents a key step in the mevalonic acid-mediated biosynthesis of isopentenyl diphosphate and other polyisoprenoid metabolites. Disruption of the PMK-encoding gene in yeast (*1*) has demonstrated the essentiality of this enzyme. Enzyme activity was documented in pig liver (*2*), and initial characterization work employed the purified porcine enzyme (*3*, *4*). The sequence of human PMK has been deduced (*5*), and expression of a recombinant GST−human PMK fusion construct (*6*) produced protein that was used to test the site of feedback inhibition of the cholesterogenic pathway.

Analysis of the rapidly expanding genomic database indicates that animal PMKs and low-homology invertebrate PMKs are encoded by genes that are nonorthologous to plant, fungal, and bacterial PMK genes (*7*). The recent discovery that the mevalonate pathway for isoprenoid biosynthesis is functionally critical in Gram-positive cocci (*8*) has been a prelude to expression of prokaryotic forms of the enzyme. For example, the enzymes from both *Enterococcus faecalis* (*9*) and *Streptococcus pneumoniae* (*10*) have been expressed, isolated, and partially characterized; the latter enzyme has been used for crystallization and elucidation of a protein structure (*10*). The fold of the nonorthologous bacterial protein confirms it to be a member of the GHMP kinase (Galactokinase/Homoserine kinase/Mevalonate kinase/Phosphomevalonate kinase) family.

No empirical structural information is available for the divergent animal PMK proteins. Animal/invertebrate PMKs have been predicted to be members of the nucleoside monophosphate kinase family of phosphotransferases on the basis of a large-scale analysis of phosphotransferase protein sequences (*7*, *11*, *12*). A recombinant human protein has been successfully overexpressed as an N-terminal His_6-tagged enzyme (*13*). The purified human enzyme, as well as several mutant proteins containing substitutions in the predicted Walker A P-loop, has been characterized. The results support

† This work was supported in part by NIDDK.

* Address correspondence to this author: phone 816-235-2246; fax 816-235-5595; e-mail miziorkoh@umkc.edu.

[1] Abbreviations: PMK, phosphomevalonate kinase; MVP, mevalonate 5-phosphate; MVPP, mevalonate 5-diphosphate; TNP-ATP, 2′-(3′)-*O*-(2,4,6-trinitrophenyl)adenosine 5′-triphosphate; NMP, nucleoside monophosphate; GST, glutathione S-transferase; LB, Luria−Bertani broth; MOPS, 3-(*N*-morpholino)propanesulfonic acid; DTT, dithiothreitol.

10.1021/bi701408t CCC: $37.00
Published on Web 09/29/2007

the assignment of human PMK to the nucleoside monophosphate (NMP) kinase family. This hypothesis is also compatible with the results of a recently generated homology model of human PMK (*13*).

Basic residues have been shown to play an important role in substrate binding and catalysis for a variety of NMP kinases (*14*−*17*). Considering this precedent and the charged nature of PMK's two phosphorylated substrates, basic residues appear to be attractive targets for any investigation into PMK function. This paper describes the identification of invariant basic residues in known and putative animal/invertebrate PMK proteins. These basic residues have been conservatively mutated; the mutant proteins have been expressed and purified. The mutant PMKs have been characterized by kinetic and biophysical methods and compared to the wild-type enzyme. This account presents the results of those experiments, which provide insight into active-site function of several of these conserved basic residues.

MATERIALS AND METHODS

Materials. Deoxynucleotides and Pfu DNA polymerase used for mutagenesis were purchased from Stratagene. Primers used for mutagenesis were obtained from Integrated DNA Technologies. Plasmid DNA was propagated in *Escherichia coli* JM109 cells (Promega). Reagents for plasmid DNA purification were purchased from Eppendorf (miniprep) and Qiagen (midiprep). DNA fragments were purified by agarose gel electrophoresis and isolated by use of a Qiaquick gel extraction kit (Qiagen). DNA sequencing was performed at the DNA Core Facility (University of Missouri—Columbia). For protein expression, *E. coli* BL21(DE3) cells were obtained from Novagen. Isopropyl β-D-thiogalactopyranoside (IPTG) was purchased from Research Products International Corp., Ni-Sepharose was from GE Healthcare, and imidazole was from Lancaster Synthesis Inc. 2′(3′)-*O*-(2,4,6-Trinitrophenyl)adenosine 5′-triphosphate (TNP-ATP) was obtained from Molecular Probes. Chemicals, buffers, media components, and antibiotics were purchased from Fisher Scientific. All other biochemical reagents and coupling enzymes were purchased from Sigma Chemical Co.

Syntheses of Mevalonate 5-Phosphate and Mevalonate 5-Diphosphate. The syntheses of mevalonate 5-phosphate and mevalonate 5-diphosphate have been previously reported (*18*, *19*) and are briefly summarized. Methyl 3-hydroxy-3-methyl-5-iodopentanoate was synthesized by reacting mevalonolactone with trimethylsilyl iodide, followed by diazomethane derivatization to form the methyl ester (*18*). The product was subsequently purified by silica gel chromatography. Methyl 5-phosphomevalonate was synthesized by reacting the purified methyl 3-hydroxy-3-methyl-5-iodopentanoate with an excess of tetrabutylammonium phosphate (*19*). The methyl 5-phosphomevalonate was converted to the lithium salt by passage over a Dowex 50 column (lithium form). Deesterification was accomplished by alkaline hydrolysis in 0.5 N LiOH for 20 h at 4 °C. The resulting mevalonate 5-phosphate was purified by anion-exchange chromatography on a DEAE-Sephadex A25 column. The chromatographically purified product was then analyzed and the concentration of the physiologically active *R* isomer was determined by enzymatic end-point assay. Mevalonate 5-diphosphate was synthesized in a similar manner but tetrabutylammonium pyrophosphate was used as the phosphorylation reagent and deesterification was performed after DEAE chromatography (*18*).

Mutagenesis. A full-circle PCR method, which employed a Stratagene QuikChange site-directed mutagenesis protocol, was used to generate the desired mutations. The presence of the mutation and the integrity of the remaining coding sequence were verified by DNA sequencing. Primer sequences used in the mutagenic reactions are as follows: K48M forward, 5′-CTCTCTGGTCCACTC**ATG**GAACAGTATGCTCAG-3′, and K48M reverse, 5′-CTGAGCATACTGTTC**CAT**GAGTGGACCAGAGAG-3′; K69M forward, 5′-CAGCACCTAC**ATG**GAGGCCTTTC-3′, and K69M reverse, 5′-GAAAGGCCTC**CAT**GTAGGTGCTG-3′; R73M forward, 5′-TACAAGGAGGCCTTT**ATG**AAGGACATGATCCGC-3′, and R73M reverse, 5′-GCGGATCATGTCCTT**CAT**AAAGGCCTCCTTGTA-3′; R84M forward, 5′-GAGAGGAGAAA**ATG**CAGGCTGACCCAG-3′, and R84M reverse, 5′-CTGGGTCAGCCTG**CAT**TTTCTCCTCTC-3′; R93M forward, 5′-CCAGGCTTCTTTTGC**ATG**AAGATTGTGGAGGGC-3′, and R93M reverse, 5′-GCCCTCCACAATCTT**CAT**GCAAAAGAAGCCTGG-3′; R110M forward, 5′ - CTGGTGAGTGACACA**ATG**AGAGTGTCTGACATC-3′, and R110M reverse, 5′-GATGTCAGACACTCT**CAT**TGTGTCACTCACCAG-3′; R111M forward, 5′-GTGAGTGACACACGG**ATG**GTGTCTGACATCCAG-3′, and R111M reverse, 5′-CTGGATGTCAGACAC**CAT**CCGTGTGTCACTCAC-3′; R130M forward, 5′-GTGACGCAGACGGTC**ATG**GTTGTAGCGTTGGAG-3′, and R130M reverse, 5′-CTCCAACGCTACAAC**CAT**GACCGTCTGCGTCAC-3′; R138M forward, 5′-GCGTTGGAGCAGAGC**ATG**CAGCAGCGGGGCTGG-3′, and R138M reverse, 5′-CCAGCCCCGCTGCTG**CAT**GCTCTGCTCCAACGC-3′; R141M forward, 5′-CAGAGCCGACAGCAG**ATG**GGCTGGGTGTTCACG-3′, and R141M reverse, 5′-CGTGAACACCCAGCC**CAT**CTGCTGTCGGCTCTG-3′.

Protein Expression. Chemically competent *E. coli* BL21(DE3) Rosetta cells were transformed with the pET15b(+) plasmid that encodes either human WT or mutant phosphomevalonate kinase containing an N-terminal His_6 affinity tag. In our initial report on this recombinant enzyme (*13*), we indicated that a C-terminal His-tagged form of PMK was also constructed, expressed, and characterized. It is comparable in activity and K_m values to the N-tagged enzyme, so no influence of the N-tag is apparent. The transformed cells were plated onto LB agar containing ampicillin (amp) and chloramphenicol (cam). These plates were incubated overnight at 37 °C. LB-amp-cam (2 mL) was inoculated with a single colony and allowed to grow to moderate turbidity (A_{600} ∼ 0.3). This culture was used to inoculate 10 LB-amp-cam plates (100 μL/plate). The plates were incubated overnight at 37 °C. The resulting lawns were used to inoculate 500 mL of LB-amp-cam (A_{600} ∼1.0). The liquid culture was incubated at 30 °C for 1 h prior to induction with 1 mM IPTG. The culture was harvested 4 h postinduction (A_{600} ∼ 2.0) by centrifugation.

Enzyme Purification. Bacterial pellets were resuspended in 100 mL of buffer containing 50 mM KP_i, 100 mM KCl, 5 mM imidazole, and 0.5 mM DTT at pH 7.8. Lysis was accomplished by passage through a microfluidizer at ∼17 kpsi. The lysate was clarified by centrifugation at ∼100000*g* and the supernatant was loaded onto ∼0.5−1.0 mL of Ni-

Sepharose Fast Flow resin. The column was washed with lysis buffer until $A_{280} < 0.005$, and the protein was eluted with lysis buffer supplemented with 300 mM imidazole. The fractions containing PMK were pooled and the concentration was determined spectrophotometrically by use of an extinction coefficient ($\epsilon_{280} = 32\,290\ M^{-1}\ cm^{-1}$) calculated from the deduced protein composition.

Steady-State Kinetics. For measurement of enzyme activity, a coupled enzyme assay was employed (*20*, *21*). In the forward reaction, initial velocities were determined by coupling the production of ADP to the oxidation of NADH with pyruvate kinase/lactate dehydrogenase (6 units/assay), and the rate of decrease in absorbance at 340 nm was monitored. In the reverse reaction, activity was determined by coupling the production of ATP to the reduction of $NADP^+$ with hexokinase/glucose 6-phosphate dehydrogenase (3 units/assay) and the rate of increase in absorbance at 340 nm was monitored. All assays were done at 30 °C in the presence of 100 mM MOPS, 200 mM KCl, 1 mM DTT, and 10 mM $MgCl_2$ at pH 7.0. Spectrophotometric measurements were performed on a Lambda 35 spectrophotometer (Perkin-Elmer). Catalytically impaired mutants were assayed fluorometrically with an excitation wavelength of 340 nm, and the rate of change in NADH or NADPH fluorescence was monitored (emission wavelength of 460 nm) on a Photon Technologies International spectrofluorometer. The activity of WT PMK was also determined fluorometrically and was in good agreement with the activity measured spectrophotometrically. All assays were started with the addition of mevalonate 5-phosphate in the forward reaction and mevalonate 5-diphosphate in the reverse reaction. For estimates of maximum velocity (V_{max}) and Michaelis constant (K_m), the reaction velocities at various substrate concentrations were fit to the Michaelis−Menten equation by use of the Kaleidagraph Graphing and Data Analysis Software (Synergy Software, Reading, PA). One unit of activity corresponds to 1 μmol of substrate converted to product in 1 min.

TNP-ATP Binding to Wild-Type and Mutant PMK Proteins. The recombinant wild-type and mutant enzymes were tested for active-site structural integrity by use of TNP-ATP, a fluorescent analogue of ATP. TNP-ATP was titrated into buffer alone or into buffer containing a fixed concentration of enzyme. The buffer used for these fluorescence measurements was 100 mM MOPS, 100 mM KCl, and 1 mM DTT at pH 7.0. Excitation wavelength used in these experiments was 409 nm. Emission spectra were scanned from 500 to 600 nm, with a 5 nm slit width. TNP-ATP concentration was determined by absorbance at 409 nm with the extinction coefficient 26 400 $M^{-1}\ cm^{-1}$ (*22*). For data analysis, values measured at the fluorescent emission peak (533−535 nm) for bound probe were corrected for free TNP-ATP/buffer. Thus, these corrected fluorescence enhancement data were plotted against TNP-ATP concentrations and analyzed by nonlinear regression to yield the ligand concentration required for half-saturation ($S_{1/2}$) and an extrapolated maximum binding (B_{max}) by use of Kaleidagraph Graphing and Data Analysis Software (Synergy Software, Reading, PA). Binding stoichiometries were determined by Scatchard analysis.

Product Inhibition of WT and Mutant PMKs. For inhibition by mevalonate 5-diphosphate, initial velocities were determined by the spectrophotometric assay. The concentration of the variable substrate, mevalonate 5-phosphate, used in these assays was 42−105 μM for WT, 204−1021 μM for R84M, and 95−1235 μM for R111M. The ATP concentration was kept constant and saturating. The concentration of the inhibitor, mevalonate 5-diphosphate, was 70−150 μM for WT, 1270−3505 μM for R84M, and 731−2194 μM for R111M. These data were fit to a competitive inhibition model by use of SigmaPlot 10.0/Enzyme Kinetics Module 1.3 (Systat Software, Inc.).

Determination of an Equilibrium Dissociation Constant for ATP by Intrinsic Tryptophan Fluorescence. All fluorescence measurements were performed on a Photon Technologies International spectrofluorometer. Intrinsic tryptophan fluorescence of WT (0.20−0.33 μM) and R141M (0.28−0.66 μM) was measured at 25 °C in 1.7 mL of buffer (100 mM Tris-HCl, 100 mM KCl, and 1 mM DTT at pH 7.5). The concentration of $MgCl_2$ in these assays was 20 and 31 mM for WT and R141M, respectively. Samples were excited at 295 nm and the emission was monitored between 310 and 450 nm. For data analysis, values measured at the fluorescent emission peak of ~333 nm were corrected for buffer background fluorescence and for dilution. Thus, these corrected fluorescence data were plotted against ATP concentrations, analyzed by nonlinear regression, and fit to a two-site model by use of GraphPad Prism version 4.00 for Windows (GraphPad Software, San Diego CA; www.graphpad.com). The K_d estimates reflect the average of three separate titrations, done at three different protein concentrations.

RESULTS

Rationale for Functional Investigation of Conserved Basic Phosphomevalonate Kinase Residues That Contribute to Active-Site Function. No empirical structural information for animal or invertebrate PMK is available. The crystal structure of the nonorthologous *S. pneumoniae* phosphomevalonate kinase has been determined (*10*) but offers little insight into animal/invertebrate PMKs. Several different groups have suggested that the animal/invertebrate enzyme belongs to the nucleoside monophosphate kinase family of enzymes (*7*, *11*−*13*). Given this information and also these constraints, 13 protein sequences of known/putative animal/invertebrate PMKs were obtained from public databases. A sequence alignment was generated by use of the BioEdit program (*23*). On the basis of this alignment, 14 basic residues (K17, R18, K19, K22, K48, K69, R73, R84, R93, R110, R111, R130, R138, and R141) were determined to be absolutely conserved (Figure 1.). Residues 17−19 and 22 are part of an atypical basic-rich "Walker A" P- loop and have been previously mutated and functionally evaluated (*13*). For NMP kinase fold enzymes, there is strong precedent for important functional contributions from basic residues outside the P-loop sequence (*14*, *16*, *24*−*26*) These observations suggested the utility of functional tests of the remaining invariant basic residues. The basic side chains of these residues have been replaced by conservative mutations to methionine; the mutant proteins have been expressed and isolated in highly purified forms (Figure 2.)

Kinetic Characterization of Human Phosphomevalonate Kinase Mutants. Three of the 10 mutant proteins (R93M, R130M, and R138M) displayed no major change in either apparent K_m (<5-fold) or V_{max} (<10-fold) values for either

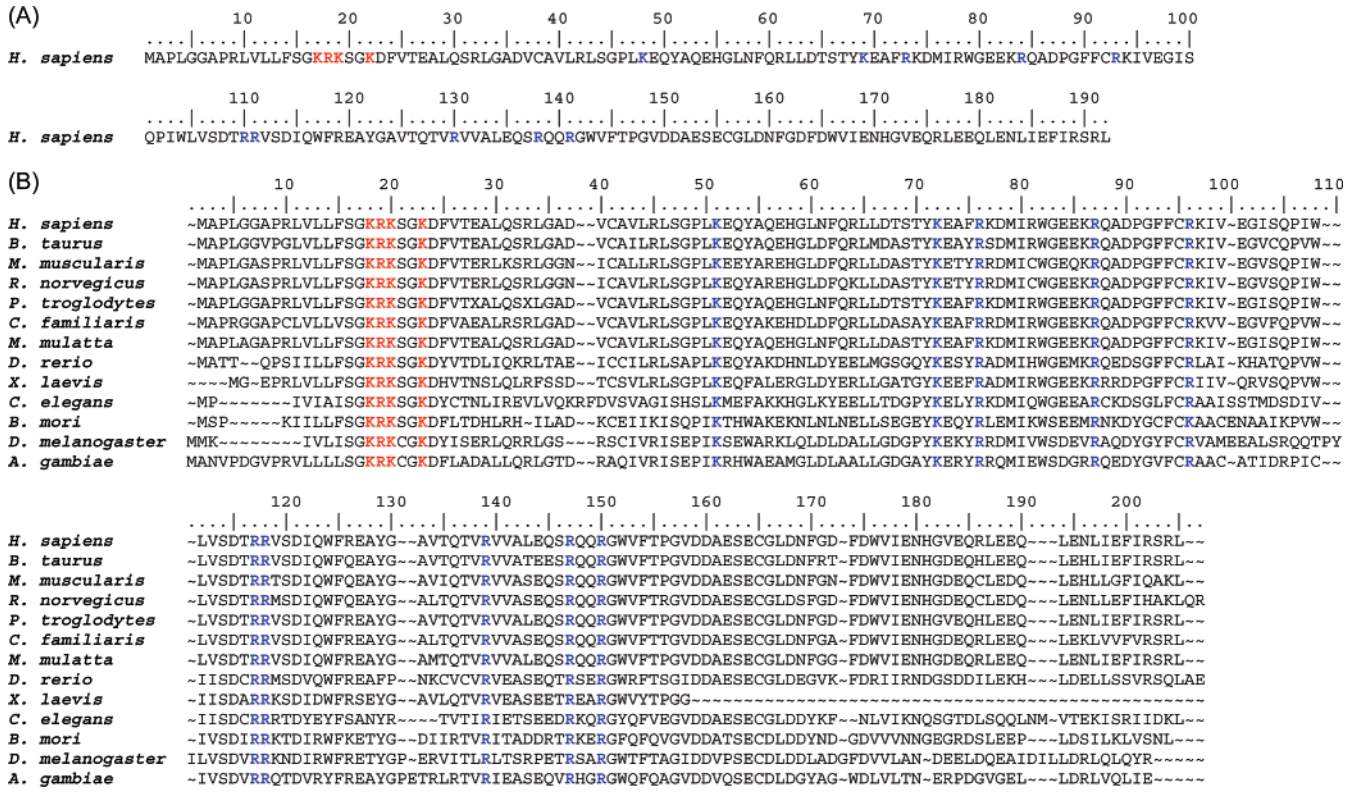

FIGURE 1: Phosphomevalonate kinase sequences. (A) The amino acid sequence of *Homo sapiens* (human) phosphomevalonate kinase is shown and the residues are numbered to correspond to the text. Conserved basic residues mutated in this study are shown in blue. Conserved basic residues previously mutated and evaluated (positions 17−19 and 22) are shown in red (*13*). (B) Sequence alignment of animal/invertebrate phosphomevalonate kinases. Conserved basic residues mutated in this study are shown in blue Conserved basic residues previously mutated and evaluated (positions 18−20 and 23) are shown in red (*13*). All sequences were obtained from public databases. Alignment was generated by use of the BioEdit program (*23*). Sequences correspond to the following organisms and accession numbers: *H. sapiens* (human), Q15126; *Bos taurus* (bovine), Q2KIU2; *Mus musculus* (mouse), Q9D1G2; *Rattus norvegicus* (rat), NP_001008353; *Pan troglodytes* (chimpanzee), XP_513842; *Canis familiaris* (dog), XP_855082; *Macaca mulatta* (rhesus monkey), XP_001114509; *Danio rerio* (zebra fish), XM_680509.1 *Xenopus laevis* (African clawed frog), NP_001089752; *Caenorhabditis elegans* (flatworm), CAD66220; *Bombyx mori* (domestic silkworm), BAF62110; *Drosophila melanogaster* (fruit fly), AAF53833; *Anopheles gambiae* (African malaria mosquito), XP_310779.

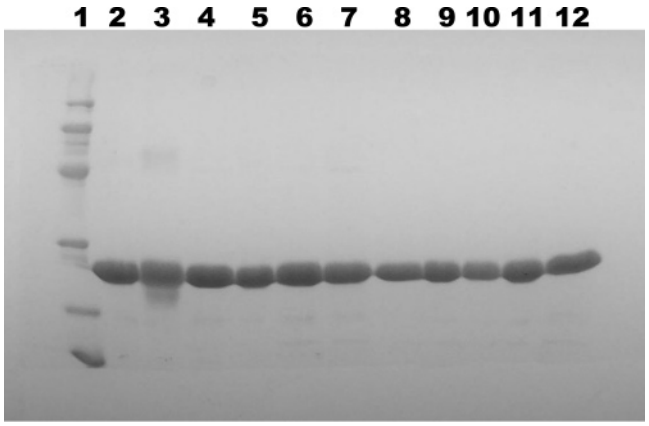

FIGURE 2: SDS−PAGE of wild-type and mutant human PMKs. Lane 1 contains molecular mass markers (phosphorylase *b*, 97.4 kDa; bovine serum albumin, 66.2 kDa; ovalbumin, 45 kDa; carbonic anhydrase, 31 kDa; trypsin inhibitor, 21.5 kDa; lysozyme, 14.4 kDa). Lanes 2−12 contain 10 μg of human PMK proteins corresponding to wt, K48M, K69M, R73M, R84M, R93M, R110M, R111M, R130M, R138M, and R141M, respectively.

the forward (Table 1) or reverse (Table 2) reactions. Substitution to eliminate the positively charged side chain resulted in a moderate to large decrease in catalysis (V_{max}) for three of the mutants: K48M (forward ~1300-fold; reverse ~1200-fold), K69M (forward ~450-fold; reverse ~1100-fold), and R73M (forward ~2600-fold; reverse ~2300-fold). The perturbation in the observed K_m for substrates in either forward or reverse reactions was minimal for the K48M, K69M, and R73M mutants (<6-fold).

Two of the PMK mutants (R84M and R111M) are clearly characterized by a substantial inflation in the apparent K_m for the nonnucleotide substrates [mevalonate 5-phosphate, 50- and 60-fold, respectively (Table 1); mevalonate 5-diphosphate, 38- and 30-fold, respectively (Table 2)]. While the R84M protein exhibited only modest effects (decreases) in V_{max} (~8-fold for forward reaction; ~21-fold for reverse reaction), R111M was more catalytically impaired in both reaction directions (forward, ~53-fold; reverse, ~86-fold).

In contrast with those K_m effects on mevalonate 5-phosphate and mevalonate 5-diphosphate, R141M is most clearly characterized by a significantly inflated apparent K_m for the nucleotide substrates [forward (ATP) ~50-fold (Table 1); reverse (ADP) ~120-fold (Table 2)]. There was little effect on V_{max} for the R141M mutation (forward reaction ~10-fold; reverse reaction ~14-fold) or on K_m (<7-fold) for nonnucleotide substrates. Estimates of K_m values for the R110M mutant PMK were precluded by the diminished activity of this mutant. Use of a more sensitive spectrofluorometric assay provided a specific activity estimate for R110M in forward and reverse reactions but not accurate measurements at subsaturating substrate concentrations. A

Table 1: Steady-State Kinetic Constants of Wild-Type and Mutant PMKs Determined for the Forward Reaction[a]

enzyme	$K_{m(R\text{-}MVP),app}$ (μM)	$V_{max(R\text{-}MVP)}$ (units/mg)	$K_{m(ATP),app}$ (μM)	$V_{max(ATP)}$ (units/mg)
WT[b]	34 ± 3	46.4 ± 1.0	107 ± 14	52.0 ± 1.1
K48M	131 ± 7	0.036 ± 0.001	236 ± 16	0.035 ± 0.001
K69M	110 ± 8	0.11 ± 0.01	268 ± 22	0.09 ± 0.01
R73M	100 ± 8	0.018 ± 0.001	94 ± 16	0.015 ± 0.001
R84M	1710 ± 49	5.89 ± 0.04	303 ± 14	3.91 ± 0.08
R93M	48 ± 3	33.1 ± 0.8	101 ± 6	32.4 ± 0.5
R110M[c]	nd	nd	nd	0.0026 ± 0.0007
R111M	2040 ± 225	0.95 ± 0.04	792 ± 102	0.69 ± 0.03
R130M	102 ± 9	14.8 ± 0.4	229 ± 16	13.2 ± 0.3
R138M	47 ± 7	17.4 ± 0.6	518 ± 61	19.9 ± 0.8
R141M[d]	225 ± 23	3.2 ± 0.1	5200 ± 474	3.6 ± 0.1

[a] Spectrophotometric assays were performed in 100 mM MOPS, 200 mM KCl, and 1 mM DTT (pH 7.0) in the presence of 10 mM $MgCl_2$ at 30 °C. Values were determined by fitting data to a Michaelis−Menten equation. Errors represent the standard error of the fit. [b] Reference *13*. [c] Specific activity determination under standard conditions by a fluorescent assay under the same buffer conditions. Error represents the standard deviation of five measurements. nd, not determined. [d] Assay contained 20 mM $MgCl_2$.

Table 2: Steady-State Kinetic Constants of Wild-Type and Mutant PMKs Determined for the Reverse Reaction[a]

enzyme	$K_{m(R\text{-}MVPP),app}$ (μM)	$V_{max(R\text{-}MVPP)}$ (units/mg)	$K_{m(ADP),app}$ (μM)	$V_{max(ADP)}$ (units/mg)
WT[b]	41 ± 3	11.3 ± 0.2	47 ± 5	12.0 ± 0.2
K48M	7 ± 1	0.0099 ± 0.0001	60 ± 6	0.0079 ± 0.0002
K69M	44 ± 3	0.0104 ± 0.0002	106 ± 10	0.009 ± 0.001
R73M	41 ± 7	0.0052 ± 0.0003	118 ± 20	0.0041 ± 0.0002
R84M	1550 ± 112	0.58 ± 0.02	238 ± 10	0.52 ± 0.01
R93M	45 ± 2	4.8 ± 0.5	91 ± 4	4.83 ± 0.06
R110M[c]	nd	nd	nd	0.000 19 ± 0.000 05
R111M	1250 ± 91	0.14 ± 0.01	93 ± 11	0.062 ± 0.002
R130M	102 ± 6	3.60 ± 0.06	164 ± 12	3.58 ± 0.06
R138M	57 ± 4	6.8 ± 0.2	451 ± 41	6.9 ± 0.2
R141M[d]	139 ± 7	0.95 ± 0.02	5620 ± 1260	1.2 ± 0.1

[a] Spectrophotometric assays were performed in 100 mM MOPS, 200 mM KCl, and 1 mM DTT (pH 7.0) in the presence of 10 mM $MgCl_2$ at 30 °C. Values were determined by fitting data to a Michaelis−Menten equation. Errors represent the standard error of the fit. [b] Reference *13*. [c] Specific activity determination under standard conditions by a fluorescent assay under the same buffer conditions. Error represents the standard deviation of six measurements. nd, not determined. [d] Assay contained 20 mM $MgCl_2$.

major diminution in the specific activity is observed in both forward (1.9×10^4-fold; Table 1) and reverse (6.3×10^4-fold; Table 2) reactions.

Evaluation of Active-Site Integrity. In view of the large catalytic effect on R110M and the substantial $K_{m,ATP}$ effect on R141M, it seemed important to ensure that these introduced mutations have not significantly perturbed the overall structure of the enzymes. For this reason, the interaction of the fluorescent ATP analogue TNP-ATP with WT, R110M, and R141M proteins was compared. It has been previously shown that the TNP-ATP, an alternative substrate for PMK, binds efficiently to the WT protein, producing enhanced fluorescence with a concomitant "blue shift" in the emission maximum (*13*). The TNP-ATP probe also binds to the most catalytically impaired mutant enzyme (R110M) and to the mutant PMK (R141M) that has the most significant perturbation in K_m for the nucleotide substrates. Analysis of the data from titration of these proteins with TNP-ATP suggests that there are no major differences in the binding stoichiometries (0.8−1.2 per site) or in equilibrium binding constants (2.3−3.9 μM) between WT and these mutant proteins (Figure 3; Table 3). For these mutants that exhibit the largest contrast with wild-type PMK in terms of kinetic parameters, the TNP-ATP data suggest that the ATP binding sites remain largely intact. Thus, these proteins exhibit no major structural perturbations that might complicate straightforward interpretation of kinetic characterization results.

Product Inhibition of Wild-Type and Mutant PMKs. To provide a test of whether the inflation in the apparent K_m values for mevalonate 5-diphosphate (Table 2) measured for R84M (38-fold) or R111M (30-fold) mutant proteins is primarily due to weakened binding of the nonnucleotide substrates, mevalonate 5-diphosphate inhibition constants were determined for the wild-type enzyme and these mutant PMKs. The data obtained from inhibition of the forward reaction by the product, mevalonate 5-diphosphate, were fit to a competitive inhibition pattern (Figure 4), so K_i comparisons should primarily reflect differences in binding affinity. The inhibition constants for WT, R84M, and R111M were estimated to be 18 μM, 1140 μM, and 806 μM, respectively (Table 4). The inflation in the inhibition constants for R84M and R111M, when compared to wild-type PMK, is 63- and 45-fold, respectively. These data correlate reasonably well with the changes in K_m for mevalonate 5-diphosphate. The combined observations strongly suggest that R84M and R111M significantly contribute to the binding of PMK's nonnucleotide substrates.

Determination of an Equilibrium Dissociation Constant for ATP by Intrinsic Tryptophan Fluorescence. For the R141M mutant, apparent K_m values for the nucleotide substrates are inflated by ~50-fold (ATP) and ~120-fold (ADP) (Tables 1 and 2). To test whether this inflation in the apparent K_m values reflects weakened binding of the nucleotide substrate, an independent estimate of nucleotide binding was pursued. Human PMK contains five tryptophan residues

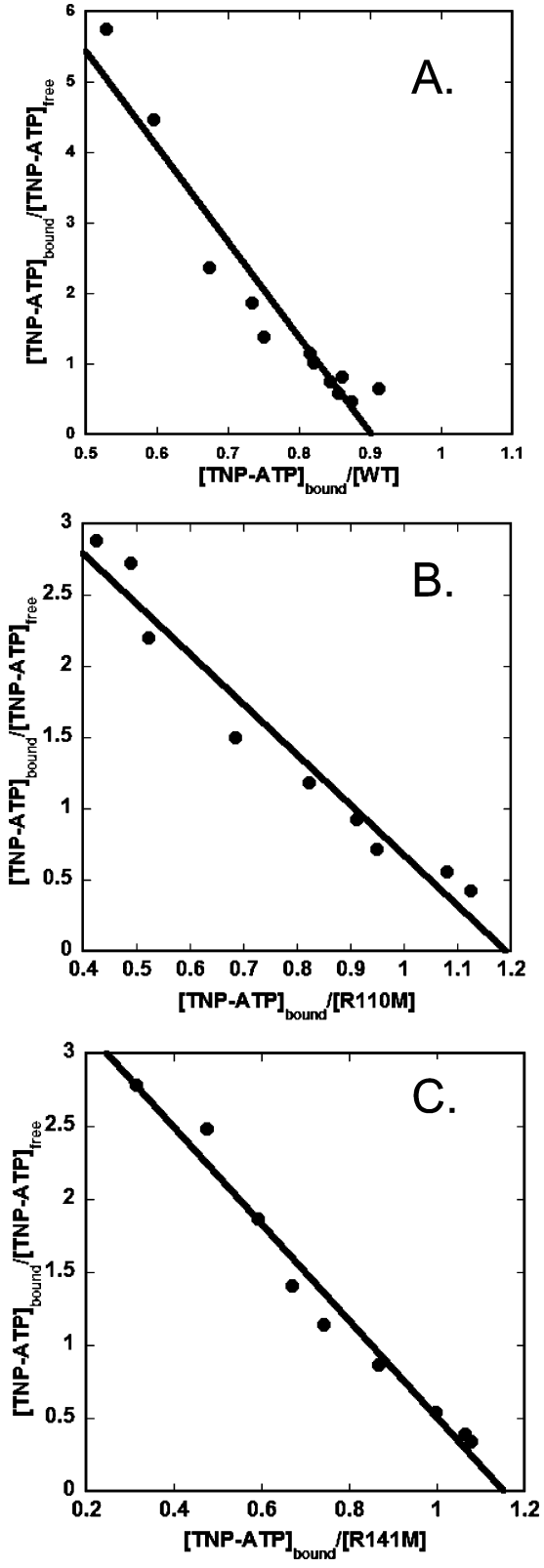

FIGURE 3: Scatchard analysis of TNP-ATP binding to wild-type and mutant human PMKs: (A) wild-type PMK; (B) R110M; (C) R141M. Conditions for binding measurements are described under Materials and Methods and in Table 3.

(W79, W104, W117, W143, and W166) (Figure 1). Two of these tryptophan residues, based on an extended protein sequence alignment of many phosphotransferases (*12*), lie in regions expected to interact with the nucleotide substrate. W104 is four residues upstream of the predicted Walker B

Table 3: Comparison of TNP-ATP Binding to Wild-Type and Mutant PMKs[a]

enzyme	$S_{1/2}$[b] (μM)	n[c]
WT	2.3 ± 0.2	0.9
R110M	3.1 ± 0.1	1.2
R141M	3.9 ± 0.2	1.2

[a] Fluorescent titrations were performed in 100 mM MOPS, 100 mM KCl, and 1 mM DTT (pH 7.0) at 25 °C. [b] $S_{1/2}$ ([ligand] at half-maximal binding) values were estimated by fitting the titration data to the nonlinear regression equation $y = B_{max}[X]/(S_{1/2} + [X])$. Errors represent the standard error of the fit. [c] The *n* value (binding stoichiometry) was estimated by Scatchard analysis.

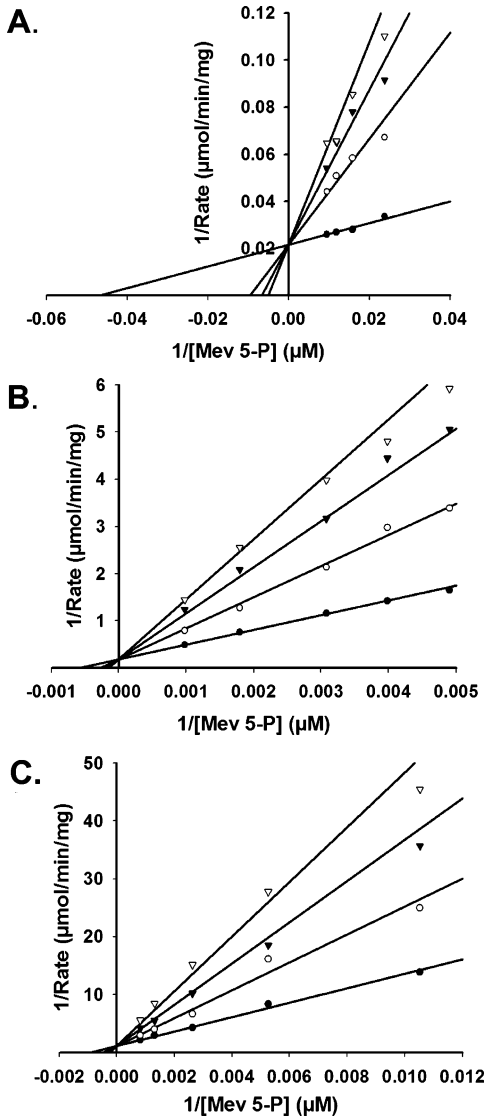

FIGURE 4: Product inhibition of wild-type and mutant human PMKs. Double-reciprocal plots of the initial velocity for PMK formation of ADP as a function of mevalonate 5-phosphate concentration, measured at different levels of the product inhibitor mevalonate 5-diphosphate, are shown. Data were fit to a competitive inhibition model by use of SigmaPlot 10.0/Enzyme Kinetics 1.3 (Systat Software, Inc.). (A) Product inhibition for wild-type PMK at (●) 0.0, (○) 0.07, (▼) 0.11, and (▽) 0.15 mM MVPP. (B) Product inhibition for R84M PMK at (●) 0.0, (○) 1.27, (▼) 2.44, and (▽) 3.50 mM MVPP. (C) Product inhibition for R111MPMK at (●) 0.0, (○) 0.73, (▼) 1.46, and (▽) 2.19 mM MVPP.

carboxylate (D108) that would be expected to interact with the divalent cation of the metal·ATP complex. W143 is two residues downstream from the mutated residue (R141). R141

Table 4: Comparison of Michaelis Constants and Product Inhibition Constants of Mevalonate Diphosphate for Wild-Type and Mutant PMKs[a]

enzyme	$K_{m(R\text{-}MVPP)}$ (μM)	*x*-fold inflation	$K_{i(R\text{-}MVPP)}$[b] (μM)	*x*-fold inflation
WT	41 ± 3		18 ± 1	
R84M	1550 ± 112	38	1140 ± 51	63
R111M	1250 ± 91	30	806 ± 85	45

[a] Spectrophotometric assays were performed in 100 mM MOPS, 200 mM KCl, and 1 mM DTT (pH 7.0) in the presence of 10 mM $MgCl_2$ at 30 °C. [ATP] was kept saturating at 5 mM. Errors represent the standard error of the fit. [b] [R-MVPP] ranged from 1 to 5 times K_i values. K_i values were estimated by fitting the data to a competitive inhibition model by use of the equation V (velocity) = $V_{max}[X]/(K_m(1 + [I]/K_i) + [X])$.

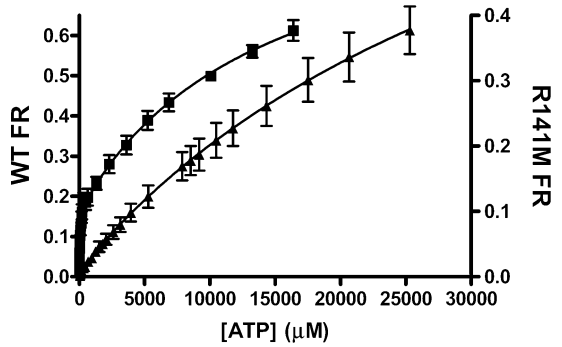

FIGURE 5: Tryptophan fluorescence quenching of WT and R141M PMK by ATP. The average fractional responses of three WT (■) concentrations (0.20−0.33 μM) and three R141M (▲) concentrations (0.28−0.66 μM) are plotted as a function of ATP concentration. All measurements were done at 25 °C in 1.7 mL 100 mM Tris-HCl, 100 mM KCl, and 1 mM DTT at pH 7.5. The concentration of $MgCl_2$ in these assays was 20 and 31 mM for WT and R141M, respectively. Samples were excited at 295 nm and the emission was monitored between 310 and 450 nm. For data analysis, values measured at the fluorescent emission peak of ~333 nm were corrected for buffer background fluorescence and for dilution. These data were analyzed by nonlinear regression and fit to a two-site model [$y = B_{max1}[X]/(K_{d1} + [X]) + B_{max2}[X]/(K_{d2} + [X])$] by use of GraphPad Prism version 4.00 for Windows (GraphPad Software, San Diego, CA; www.graphpad.com). Error bars represent the standard deviation of the three different protein concentrations.

aligns with residues from several NMP kinases known to be in the "lid" domain. A conserved arginine in this region of the NMP kinase "lid" has been implicated in formation of a critical interface with the adenine moiety of ATP in thymidylate, shikimate, gluconate, and dephospho-coenzyme A kinases(*27*−*30*). On this basis, it seemed reasonable to test whether ATP influences PMK tryptophan fluorescence.

For both wild-type and R141M PMK (which exhibits a substantial inflation of K_m for nucleotide substrates), tryptophan fluorescence data were measured as a function of ATP concentration (Figure 5). The data were best fit to a two-site binding equation to estimate the ATP equilibrium dissociation constants for WT and R141M PMKs. The dissociation constants for the first (tight) site for WT and R141M were estimated to be 30 μM and 816 μM, respectively (Table 5). When compared to corresponding parameters for wild-type PMK, the inflation in K_{d1} (~27-fold) correlates reasonably well the inflation in the apparent $K_{m,ATP}$ (~49-fold). These observations suggest that R141 plays a role in the binding of the nucleotide substrates. Second (weak) site dissociation constants for WT and R141M PMK proteins were estimated to be 14 mM and 41 mM, respectively. These second-site binding constants are well above the physiological concentration of ATP and were not considered for further analysis.

Table 5: Comparison of Michaelis Constants and Equilibrium Binding Constants for ATP to Wild-Type and Mutant PMKs[a]

enzyme	$K_{m(ATP)}$ (μM)	*x*-fold inflation	$K_{d(ATP)}$[b] (μM)	*x*-fold inflation
WT	107 ± 14		30 ± 3	
R141M	5200 ± 474[c]	49	816 ± 160	27

[a] Spectrophotometric assays were performed in 100 mM MOPS, 200 mM KCl, and 1 mM DTT (pH 7.0) in the presence of 10 mM $MgCl_2$ at 30 °C. [ATP] was kept saturating (5 mM). Errors represent the standard error of the fit. [b] Determined by tryptophan fluorescence. Averaged data points from three [protein] were fit to a two-site model by use of the equation $y = B_{max1}[X]/(K_{d1} + [X]) + B_{max2}[X]/(K_{d2} + [X])$. K_{d2} values (WT 14 mM, R141M 41 mM) are too weak to be physiologically relevant and are not considered in the comparison. Errors represent the standard error of the fit. [c] Assays contained 20 mM $MgCl_2$.

DISCUSSION

Nucleoside monophosphate kinase family proteins include numerous examples of phosphoryl transfer between two nucleotides [e.g., dexoynucleotide kinase (*31*), adenylate kinase (*14*−*17*), thymidylate kinase (*30*), etc.] or between a nucleotide and the alcohol group of a nonnucleotide acceptor metabolite [e.g., 6-phosphofructo-2-kinase (*24*), phosphoribulokinase (*25*), shikimate kinase (*28*), gluconate kinase (*27*)]. Phosphomevalonate kinase is unusual in this family of proteins in that it catalyzes a phosphoryl transfer from a nucleotide donor (ATP) to the phosphate of a nonnucleotide metabolite acceptor (mevalonate 5-phosphate). Several limitations to analysis of the protein include the lack of a structure of the animal/invertebrate enzyme as well as the divergence of yeast and lower PMK proteins from the NMP kinase family fold. Nevertheless, the reported sequences of animal and invertebrate PMK proteins have recently grown to an appreciable number and it has been possible to identify a manageable number of conserved basic residues and to test their potential function. Fortunately, when charged side chains of basic residues were eliminated by a methionine substitution, the resulting mutant proteins could be expressed and isolated in a fashion comparable to wild-type enzyme, allowing pursuit of the functional analyses reported under Results. Of six mutants (K48M, R73M, R84M, R110M, R111M, and R141M) that exhibit substantial diminution in k_{cat} or inflation in substrate K_m (Tables 1 and 2), reasonable functional explanations are possible for most of these and are summarized below.

In the case of PMK's R110, this residue is only two residues downstream of the putative "Walker B" carboxyl [IWLVS**D$_{108}$** (*12*)] that typically binds a cation of the M^{2+}-ATP substrate. Deoxynucleotide kinase (*31*) also exhibits such a motif, but the functional test of the comparable arginines has only been reported in this work on PMK. Ostermann et al. (*30*) have proposed that, for thymidylate kinase, a basic residue near a Walker B motif bridges

phosphoryl donor and acceptor substrates. In such a case, the basic side chain (e.g., PMK R110's guanidinium group) could be critical in affecting the proximity and alignment of substrates, so the large k_{cat} effect ($\sim 10^4$-fold decrease in specific activity) would be compatible with such a role in catalysis.

R111 in PMK is also close to the "Walker B" motif and, since phosphoryl acceptor must be situated in close proximity to allow efficient in-line phosphoryl transfer from the donor to occur, it is reasonable that mevalonate 5-phosphate's K_m (Table 1) or mevalonate 5-diphosphate's K_m (Table 2) would be affected if R111's guanidinium group is substituted. Similar inflations of K_m for the phosphoryl acceptor in the NMP kinase family enzymes phosphoribulokinase (*32*) and 6-phosphofructo-2-kinase (*26*) occur upon arginine mutagenesis. Thus, the prediction that R111 supports binding of PMK's nonnucleotide substrate seems reasonable, especially since the product inhibition data (Table 4) for R111M confirm the inflation observed in K_m for mevalonate 5-phosphate and mevalonate 5-diphosphate.

In considering residues that are not so easily associated with established sequence motifs and reinforced by some defined regions in a PMK homology model (*13*), reliance on large-scale phosphotransferase sequence alignments can provide some insight. For example, PMK R141 falls into the $RX_{(2-3)}R$ sequence commonly observed in the "lid" region of NMP kinases. Basic residues in this sequence have been proposed to interact with the substrate adenine moiety (*12*). PMK's R141 could function in such a capacity. This would explain R141M's dominant effects on apparent nucleotide affinity, with contrasting observations of large K_m effects for ATP and ADP ($\sim$50−100-fold) but more modest effects on K_m for nonnucleotide substrates.

Finally, in considering PMK's K48M, which exhibits a significant ($>10^3$-fold) effect on k_{cat} but little effect on K_m of any substrate, it may be useful to note the homology to CMP kinase's R41 (*12*). R41 in CMP kinase (*33*) hydrogen-bonds to the α-phosphoryl of CMP, which is the acceptor substrate in the CMP kinase reaction. If PMK's K48 should support a similar function, substitution of its charged side chain (e.g., K48M) could disrupt PMK's ability to precisely orient the acceptor with respect to the donor γ-phosphoryl of ATP. For such a function, a k_{cat} effect of the magnitude observed for K48M would be quite reasonable.

REFERENCES

1. Tsay, Y. H., and Robinson, G. W. (1991) Cloning and characterization of ERG8, an essential gene of *Saccharomyces cerevisiae* that encodes phosphomevalonate kinase, *Mol. Cell. Biol. 11*, 620−631.
2. Hellig, H., and Popjak, G. (1961) Studies on the biosynthesis of cholesterol: XIII. Phosphomevalonic kinase from liver, *J. Lipid Res. 2*, 235−243.
3. Bazaes, S., Beytia, E., Jabalquinto, A. M., Solis de Ovando, F., Gomez, I., and Eyzaguirre, J. (1980) Pig liver phosphomevalone kinase. 1. Purification and properties, *Biochemistry 19*, 2300−2304.
4. Lee, C. S., and O'Sullivan, W. J. (1985) Improved procedures for the synthesis of phosphomevalonate and for the assay and purification of pig liver phosphomevalonate kinase, *Biochim. Biophys. Acta. 839*, 83−89.
5. Chambliss, K. L., Slaughter, C. A., Schreiner, R., Hoffmann, G. F., and Gibson, K. M. (1996) Molecular cloning of human phosphomevalonate kinase and identification of a consensus peroxisomal targeting sequence, *J. Biol. Chem. 271*, 17330−17334.
6. Hinson, D. D., Chambliss, K. L., Toth, M. J., Tanaka, R. D., and Gibson, K. M. (1997) Post-translational regulation of mevalonate kinase by intermediates of the cholesterol and nonsterol isoprene biosynthetic pathways, *J. Lipid Res. 38*, 2216−2223.
7. Smit, A., and Mushegian, A. (2000) Biosynthesis of isoprenoids via mevalonate in Archaea: the lost pathway, *Genome Res. 10*, 1468−1484.
8. Wilding, E. I., Brown, J. R., Bryant, A. P., Chalker, A. F., Holmes, D. J., Ingraham, K. A., Iordanescu, S., So, C. Y., Rosenberg, M., and Gwynn, M. N. (2000) Identification, evolution, and essentiality of the mevalonate pathway for isopentenyl diphosphate biosynthesis in gram-positive cocci, *J. Bacteriol. 182*, 4319−4327.
9. Doun, S. S., Burgner, J. W., 2nd, Briggs, S. D., and Rodwell, V. W. (2005) *Enterococcus faecalis* phosphomevalonate kinase, *Protein Sci. 14*, 1134−1139.
10. Romanowski, M. J., Bonanno, J. B., and Burley, S. K. (2002) Crystal structure of the *Streptococcus pneumoniae* phosphomevalonate kinase, a member of the GHMP kinase superfamily, *Proteins: Struct., Funct., Genet. 47*, 568−571.
11. Houten, S. M., and Waterham, H. R. (2001) Nonorthologous gene displacement of phosphomevalonate kinase, *Mol. Genet. Metab. 72*, 273−276.
12. Leipe, D. D., Koonin, E. V., and Aravind, L. (2003) Evolution and classification of P-loop kinases and related proteins, *J. Mol. Biol. 333*, 781−815.
13. Herdendorf, T. J., and Miziorko, H. M. (2006) Phosphomevalonate kinase: functional investigation of the recombinant human enzyme, *Biochemistry 45*, 3235−3242.
14. Dahnke, T., Shi, Z., Yan, H., Jiang, R. T., and Tsai, M. D. (1992) Mechanism of adenylate kinase. Structural and functional roles of the conserved arginine-97 and arginine-132, *Biochemistry 31*, 6318−6328.
15. Tian, G. C., Yan, H. G., Jiang, R. T., Kishi, F., Nakazawa, A., and Tsai, M. D. (1990) Mechanism of adenylate kinase. Are the essential lysines essential? *Biochemistry 29*, 4296−4304.
16. Yan, H. G., Dahnke, T., Zhou, B. B., Nakazawa, A., and Tsai, M. D. (1990) Mechanism of adenylate kinase. Critical evaluation of the X-ray model and assignment of the AMP site, *Biochemistry 29*, 10956−10964.
17. Yan, H. G., Shi, Z. T., and Tsai, M. D. (1990) Mechanism of adenylate kinase. Structural and functional demonstration of arginine-138 as a key catalytic residue that cannot be replaced by lysine, *Biochemistry 29*, 6385−6392.
18. Reardon, J. E., and Abeles, R. H. (1987) Inhibition of cholesterol biosynthesis by fluorinated mevalonate analogues, *Biochemistry 26*, 4717−4722.
19. Wang, C. Z., and Miziorko, H. M. (2003) Methodology for synthesis and isolation of 5-phosphomevalonic acid, *Anal. Biochem. 321*, 272−275.
20. Liu, F., Dong, Q., Myers, A. M., and Fromm, H. J. (1991) Expression of human brain hexokinase in *Escherichia coli*: purification and characterization of the expressed enzyme, *Biochem. Biophys. Res. Commun. 177*, 305−311.
21. Tchen, T. T. (1962) Enzymes in Sterol Biogenesis, *Methods Enzymol. 5*, 489−499.
22. Hiratsuka, T., and Uchida, K. (1973) Preparation and properties of 2′(or 3′)-*O*-(2,4,6-trinitrophenyl)adenosine 5′-triphosphate, an analog of adenosine triphosphate, *Biochim. Biophys. Acta. 320*, 635−647.
23. Hall, T. A. (1999) BioEdit: A user-friendly biological sequence alignment editor and analysis program for Window 95/98/NT, *Nucleic Acids Symp. Ser. 41*, 95−98.
24. Li, L., Lin, K., Pilkis, J., Correia, J. J., and Pilkis, S. J. (1992) Hepatic 6-phosphofructo-2-kinase/fructose-2,6-bisphosphatase. The role of surface loop basic residues in substrate binding to the fructose-2,6-bisphosphatase domain, *J. Biol. Chem. 267*, 21588−21594.
25. Runquist, J. A., Harrison, D. H., and Miziorko, H. M. (1999) *Rhodobacter sphaeroides* phosphoribulokinase: identification of lysine-165 as a catalytic residue and evaluation of the contributions of invariant basic amino acids to ribulose 5-phosphate binding, *Biochemistry 38*, 13999−14005.
26. Tsujikawa, T., Watanabe, F., and Uyeda, K. (1995) Hexose phosphate binding sites of fructose 6-phosphate,2-kinase:fructose 2,6-bisphosphatase, *Biochemistry 34*, 6389−6393.

27. Kraft, L., Sprenger, G. A., and Lindqvist, Y. (2002) Conformational changes during the catalytic cycle of gluconate kinase as revealed by X-ray crystallography, *J. Mol. Biol. 318*, 1057−1069.
28. Krell, T., Coggins, J. R., and Lapthorn, A. J. (1998) The three-dimensional structure of shikimate kinase, *J. Mol. Biol. 278*, 983−997.
29. Obmolova, G., Teplyakov, A., Bonander, N., Eisenstein, E., Howard, A. J., and Gilliland, G. L. (2001) Crystal structure of dephospho-coenzyme A kinase from *Haemophilus influenzae*, *J. Struct. Biol. 136*, 119−125.
30. Ostermann, N., Schlichting, I., Brundiers, R., Konrad, M., Reinstein, J., Veit, T., Goody, R. S., and Lavie, A. (2000) Insights into the phosphoryltransfer mechanism of human thymidylate kinase gained from crystal structures of enzyme complexes along the reaction coordinate, *Structure 8*, 629−642.
31. Teplyakov, A., Sebastiao, P., Obmolova, G., Perrakis, A., Brush, G. S., Bessman, M. J., and Wilson, K. S. (1996) Crystal structure of bacteriophage T4 deoxynucleotide kinase with its substrates dGMP and ATP, *EMBO J. 15*, 3487−3497.
32. Sandbaken, M. G., Runquist, J. A., Barbieri, J. T., and Miziorko, H. M. (1992) Identification of the phosphoribulokinase sugar phosphate binding domain, *Biochemistry 31*, 3715−3719.
33. Bertrand, T., Briozzo, P., Assairi, L., Ofiteru, A., Bucurenci, N., Munier-Lehmann, H., Golinelli-Pimpaneau, B., Barzu, O., and Gilles, A. M. (2002) Sugar specificity of bacterial CMP kinases as revealed by crystal structures and mutagenesis of *Escherichia coli* enzyme, *J. Mol. Biol. 315*, 1099−1110.

BI701408T